INL/CON-23-71293-Revision-2

Response of Graphite to Dynamic Loading and Hypervelocity Jet Impacts

February 2024

Bradley Davis Huddleston, Thomas A Mason, Cody James Gibson, Colter Z Angell, Nikki Rasmussen

Changing the World's Energy Future

INL is a U.S. Department of Energy National Laboratory operated by Battelle Energy Alliance, LLC

INL/CON-23-71293-Revision-2

Response of Graphite to Dynamic Loading and Hypervelocity Jet Impacts

Bradley Davis Huddleston, Thomas A Mason, Cody James Gibson, Colter Z Angell, Nikki Rasmussen

February 2024

Idaho National Laboratory
Idaho Falls, Idaho 83415

http://www.inl.gov

Prepared for the
U.S. Department of Energy
Under DOE Idaho Operations Office
Contract DE-AC07-05ID14517

Proceedings of the ASME 2023
International Mechanical Engineering Congress and Exposition
IMECE2023
October 29-November 2, 2023, New Orleans, Louisiana

IMECE2023-111256

RESPONSE OF GRAPHITE TO DYNAMIC LOADING AND HYPERVELOCITY JET IMPACTS

Bradley D. Huddleston[1], Thomas A. Mason[1], Cody Gibson[1], Colter Angell[1], Nikki Rasmussen[1]

[1]Idaho National Lab, Idaho Falls, Idaho

ABSTRACT

The compressive strengths of three varieties of high purity graphite, PCEA, NBG-18, and NBG-25, as well as the depth of penetration of small-scale charges into these materials was experimentally determined. These grades are similar in density, ranging from 1.80 – 1.85 g/cc, and nominal apparent porosity, ranging from 18% to 20%, but provide a wide range in maximum grain or particle size from 10s to 1000s of μm. Two very different manufacturing methods are also represented; PCEA is extruded while NBG-18 and NBG-25 are iso-molded. The quasistatic and dynamic strengths of each grade were determined on a load frame and split-Hopkinson pressure bar, respectively. The depth of penetration (DOP) of two small-scale shaped charges, the Teledyne RP-1 and RP-4, was determined against graphite. The global response of the RP-4 impacts was markedly different as the PCEA samples remained intact while all the NBG-25 samples split into 2 or 3 pieces after the jet penetration had completed. However, for all tests, the trusted DOPs fell within 2 cm. Preliminary hydrocode modeling of the penetration events used existing models that were not designed for graphite. The results can be tuned to reasonably reproduce the DOP, but the wound channel geometry is not reproduced well. A model designed for graphite would need to represent graphite's non-linear and energy dissipation characteristics.

Keywords: Graphite, Dynamic Properties, Shaped Charge, Hypervelocity

NOMENCLATURE

DOP	depth of penetration
PETN	Pentaerythritol tetranitrate explosive
RDX	Royal Demolition Explosive (Cyclonite)
SHPB	Split-Hopkinson pressure bar
HEL	Hugoniot elastic limit

1. INTRODUCTION

Artificial or synthetic graphite has a unique combination of thermal, mechanical, and neutronic properties that have rendered it a prominent material for several applications. Notably, it is used in refractory applications, as an anode in certain types of batteries, and as a conductor in some electrical applications. Because of these applications, most work has focused on quantifying thermal and quasistatic mechanical properties [1, 2, 3].

A limited amount of work has been done on characterizing the dynamic properties of high purity graphite. Yokoyama *et al.* [4, 5] looked at the dynamic strength of graphite with a split-Hopkinson pressure bar (SHPB) in both compression and tension for IG-11, finding that the strength of IG-11 had very little rate sensitivity. Tian *et al.* [6] performed SHPB splitting disc tests on coarse and fine grained graphites and found that the coarse grained graphite experienced a ~60% increase in strength, while the fine grained graphite experienced only a 20% increase in strength over the quasistatic values.

Additional studies have been done on using graphite as a space radiator material, specifically on the resilience of the graphite structures to hypervelocity micrometeoroid impacts [7, 8]. Another group is exploring a similar case [9-11] using a pressured dependent yield model or a modified JH2 model for a porous POCO EDM3 graphite.

The dynamic compressive strengths of three varieties of high-purity graphite are reported. In addition, the penetration of a hypervelocity jet into graphite materials is quantified and some unique behaviors of graphite are identified. The penetration events are modeled in a hydrocode using two different material models for graphite.

2. MATERIALS AND METHODS

2.1 Graphite materials

Three graphite materials are used in this study: PCEA, NBG-18, and NBG-25. PCEA is a medium grain (760 um max. [12]) extruded graphite. The nominal porosity is 20%, though values of 16% for apparent porosity have been reported [13]. The average pore size is reported as 3.9 um, but most of porosity is due to large pores, up to 213 um.

NBG-18 is an isostatically pressed graphite with a larger grain size (1.6 mm), and a similar apparent porosity (14% [13]). The pore size distribution of NBG-18 is similar to PCEA. NBG-

25, while also isostatically pressed, has a much smaller grain size (60 um [14]). It also has a similar nominal porosity of 20% [15].

2.2 Shaped charge and test methods

Two shaped charges are used in this study, the Teledyne RP-1 and RP-4. The RP-1 (PN 188-7355) is an older, discontinued charge with a 0.410" outer diameter and 530 mg of pressed PETN. The geometry is shown in Figure 1. The RP-4 (PN 188-7377) has a 1.01" outer diameter and 3.44 g of RDX with an RP-80 booster (86 mg PETN + 123 mg RDX), and its geometry is shown in Figure 2. Both the RP-1 and RP-4 were used against PCEA graphite, while just the RP-4 was used against the NBG grades. The larger charge was deemed to provide more informative results.

An aluminum 6061-T6511 plate was used as a conditioning plate. The primary goal of the conditioning plate was to limit the amount of copper "splatter" created during the formation of the jet from impacting the graphite and reduce the total penetration into the graphite.

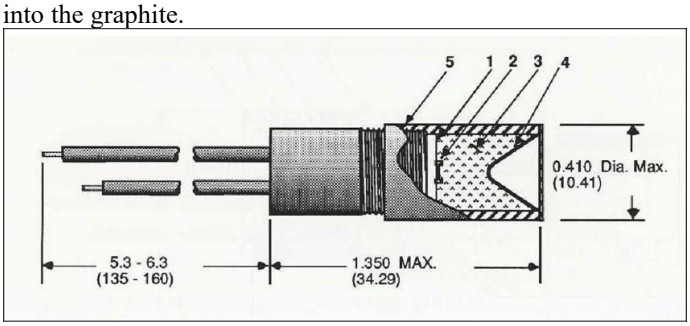

FIGURE 1: MODEL GEOMETRY FOR TELEDYNE RP-1 SHAPED CHARGE. NUMBERS INDICATE THE COMPONENTS: (1) RP-1 STANDARD DETONATOR HEAD; (2) BRIDGEWIRE: GOLD, 0.0015" DIA. 0.040" LONG; (3) 530 MG PRESSED PETN; (4) COPPER LINER; (5) BRASS SLEEVE, 0.050" THICK [16].

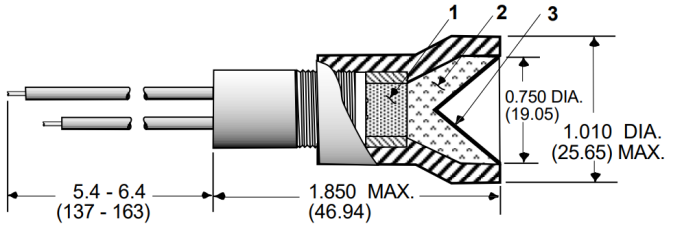

FIGURE 2: MODEL GEOMETRY FOR THE TELEDYNE RP-4 SHAPED CHARGE. NUMBERS INDICATE THE COMPONENTS: (1) RP-80 DETONATOR; (2) 2.44 G OF PLASTICIZED RDX; (3) COPPER LINER, 60 DEGREES BY 0.020" (0.0508 CM) THICK [17].

2.3 Simulation Methods

Simulations were performed in the hydrocode CTH [18]. The shaped charge jet formation events were run once and a snapshot from the appropriate timestep was imported into a simulation with the graphite target. The formation process was validated by comparing the jet tip velocities to those reported in literature [16]. The formation processes adequately matched those results, as shown in Table 1. For the RP-1, the anomalous low velocity is ignored for the purpose of validating the formation simulation.

TABLE 1: JET TIP VELOCITY AFTER FORMATION FOR RP-1 AND RP-4 SHAPED CHARGES

Charge	*Simulated Tip Velocity (km/s)*	*Ref. 16 (km/s)*
RP-1	4.31	4.87 ± 0.15, 4.24 ± 0.13
RP-4	5.37	5.31 ± 0.13

3. RESULTS AND DISCUSSION

3.1 Strength results

The compressive strengths of each grade of graphite were evaluated via quasistatic compression tests and SHPB compression tests. The quasistatic tests were run on cylindrical samples 1.27 cm (0.5") diameter by 2.54 cm (1") length at a strain rate of $1x10^{-3}$ s^{-1}. The SHPB tests were performed on cylindrical samples of 1.27 cm (0.5") diameter as aspect ratio of 1 at strain rates from 250 s^{-1} to 650 s^{-1}. The results are shown in Figure 3. The triangle markers for NBG-25 indicate tests where the sample did not fail under the applied strain pulse. For most tests, there was a slight increase in strength with strain rate, except for PCEA in the radial direction. The PCEA was tested in both the extrusion direction, and perpendicular to the extrusion direction (radial direction on the cylindrical extrusion). There was no significant difference in quasistatic strength between the axial and radial directions, but some reduction in strength was observed in the dynamic tests for the radial direction. With the limited number of samples shown, additional experiments should be run before concluding that there is a negative rate sensitivity for the radial direction PCEA.

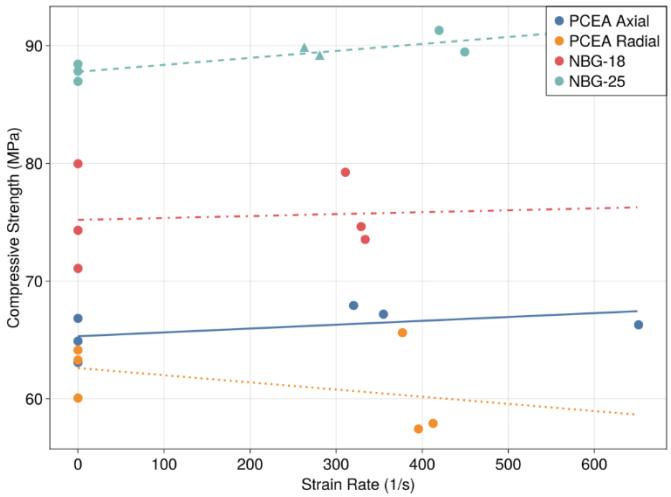

FIGURE 3: STRAIN RATE DEPENDENCE OF COMPRESSIVE STRENGTH OF GRAPHITE FROM QUASISTATIC TO SPLIT-HOPKINSON PRESSURE BAR EXPERIMENTS.

3.2 Material Model Fits

There are few existing material models designed for graphite [19, 20], and these are not implemented in CTH. Thus, two different material model setups were used to try to model the penetration events. The first used the 7830 carbon Sesame table with a P-alpha porosity model for the equation of state. The strength model was an elastically perfectly plastic model whose yield strength linearly depended on pressure. As mechanical data for high pressures or strain rates for these grades of graphite is scarce, some parameters are assumed from existing literature for different grades of graphite. The parameters for the equation of state portion of the model are shown in Table 2, and the strength portion are shown in Table 3. The source for each parameter is given by the references in the table. The pressure dependence on yield (DPDY) is taken from [9] where it was applied to POCO EDM3 graphite. While these graphite grades are likely somewhat different, the value used should be a good estimate. The yield strength in Table 2 is set to the compressive strengths reported in Section 3.1. The tensile yield for NBG-25 was estimated based on the ratio of the compressive strengths.

TABLE 2: P-ALPHA EQUATION OF STATE PARAMETERS FOR GRAPHITE

Parameter	*PCEA*	*NBG-18*	*NBG-25*
Initial density (g/cc)	1.834 [2]	1.846 [3]	1.82 [11]
Solid density (g/cc)	2.257 [14]	2.253 [14]	2.253
Compaction Pressure (GPa)	1.0 [11]	1.0 [11]	1.0 [11]
Elastic Pressure (GPa)	0.1 [11]	0.1 [11]	0.1 [11]
Elastic Sound Speed (cm/s)	252480 [2]	276600 [3]	273068 [22]

TABLE 3: MATERIAL PARAMETERS FOR GRAPHITE FOR THE GEOLOGIC YIELD MODEL

Parameter	*PCEA*	*NBG-18*	*NBG-25*
Yield (MPa)	65.3	75.2	87.8
Y0 (MPa)	18.3 [2]	19.5 [3]	22.8
Poisson Ratio	0.178 [3]	0.23 [3]	0.229 [22]
DYDP	0.076 [10]	0.076 [10]	0.076 [10]

The second material model is the Johnson-Holmquist II (JH2) ceramic material model [22]. JH2 is designed to represent the behavior of brittle materials, especially ceramics, under extreme pressures and in shock environments. The equation of state portion is a third order expansion around the volume change, $\mu = \frac{\rho}{\rho_0} - 1$, with an additional term based on the bulking pressure as the material fails.

$$P = K_1\mu + K_2\mu^2 + K_3\mu^3 + P_{Bulk} \quad (1)$$

The strength of the material is given as:

$$\sigma = (1 - D) \cdot Y_{NF} + D \cdot Y_F$$

where the non-failed strength, Y_{NF}, and the failed strength, Y_N, are:

$$Y_{NF} = \sigma_{HEL} \cdot A \cdot \left(\frac{P}{P_{HEL}} - \frac{T}{P_{HEL}}\right)^N \cdot (1 + C \ln(\dot{\varepsilon})) \quad (3)$$

$$Y_F = \min\left(\sigma_{HEL} \cdot B \cdot \left(\frac{P}{P_{HEL}}\right)^M \cdot (1 + C\, ln(\dot{\varepsilon})), SFMax\right) \quad (4)$$

Damage, D, is defined as:

$$D = \sum \frac{\dot{\varepsilon}_p}{D1 \cdot \left(\frac{P}{P_{HEL}} - \frac{T}{P_{HEL}}\right)^{D2}} \Delta t \quad (5)$$

Full details of this material model can be found in [22].

The material parameters used in this work are shown in Table 4. The initial bulk modulus, K1, was set to the bulk modulus calculated from the elastic constants. The other EOS parameters, K2, K3, are fit to approximately represent the same behavior as the P-alpha + Sesame model used in the first material model. The Hugoniot elastic limit (HEL) is used from [11], which represents a value for POCO EDM3 graphite. The value for the non-failed strength, A, is fit to the graphite compressive strengths reported in Section 3.1. A is normalized by the deviatoric stress at the HEL, σ_{HEL}, which results in the values shown. We currently have no experimental data to determine B, so it is calibrated to obtain the observed DOP. This choice precludes the predictive nature of the model for these experiments, but still allows us to evaluate whether the model can represent the experiment. The value for the strain rate sensitivity parameter, C, is taken from log-linear fits of the data in Figure 3. C is dependent on the current equivalent strain rate, $\dot{\varepsilon}$. Other values are taken from the model for POCO EDM3 graphite in [11], as indicated by the references in the table. The material parameters M and N are related to the pressure dependence of the material strength; T is the tensile failure pressure, which is negative in tension; and *SFMax* is the maximum allowed strength for failed material. The dependence of both failed and intact strength on pressure is shown in Figure 4 for each of the three materials.

TABLE 4: MATERIAL PARAMETERS FOR GRAPHITE FOR THE JOHNSON-HOLMQUIST II MODEL

Parameter	*PCEA*	*NBG-18*	*NBG-25*
K1 (GPa)	5.58	7.52	7.21
K2 (GPa)	-40	-60	-60
K3 (GPa)	170	210	210
G (GPa)	4.58 [2]	4.95 [2]	4.77 [21]
Beta	0 [11]	0 [11]	0 [11]
A	1.169	1.503	1.715
B	0.30	0.55	0.20
C	0.00252	0.000701	0.00191
M	1 [11]	1 [11]	1 [11]
N	0.6 [11]	0.6 [11]	0.6 [11]
T (MPa)	-18.3 [2]	-19.5 [2]	-22.8

HEL (MPa)	70 [11]	70 [11]	70 [11]
P_HEL (MPa)	32.77	36.65	35.87
σ_{HEL} *(MPa)*	55.85	50.02	51.20
μ_{HEL}	0.00613	0.00508	0.00520
D1	0.20	0.20	0.20
D2	0 [11]	0 [11]	0 [11]
SFMax (MPa)	600	600	600

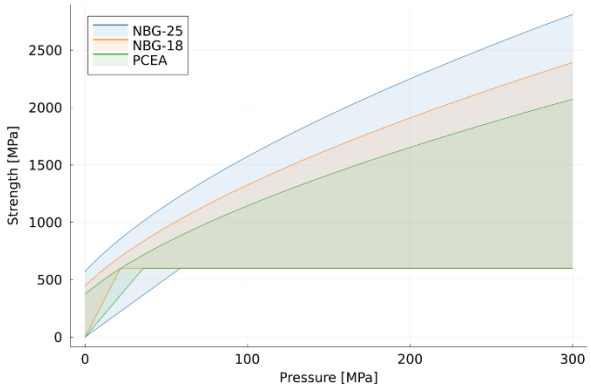

FIGURE 4: VARIATION OF STRENGTH WITH PRESSURE FOR EACH OF THE THREE GRAPHITE MATERIAL MODEL PARAMETER SETS.

3.3 Depth of Penetration Results

Two tests were performed with the RP-1, both into PCEA. The distance to target was 1.5 cm with a 0.79 cm (5/16") Al-6061 conditioner in the configuration shown in Figure 5. The front and back spacings were both 0.35 cm. The front spacing is termed the standoff as it is the distance to the first material in the jet's path.

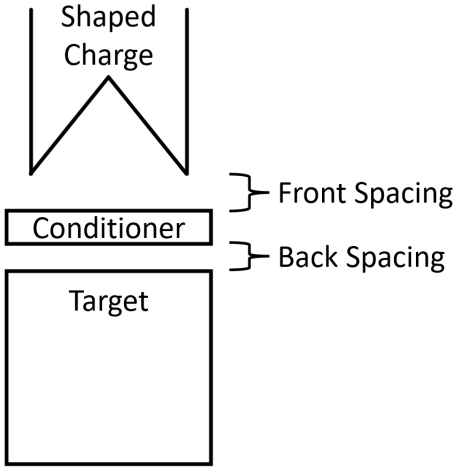

FIGURE 5: SHAPED CHARGE TEST CONFIGURATION WITH INTERMEDIATE CONDITIONER.

A total of 9 tests were performed with the RP-4, with two different test configurations. The first configuration had a conditioner thickness of 2.22 cm (7/8") and front and back spacings of 0.32 cm (1/8"). The drawback with this configuration is that the jet had a limited space to equilibrate before encountering the conditioning plate. We suspect that this compromised the effectiveness of the jet. The second configuration had a conditioner thickness of 2.54 cm (1"), a back spacing of 0.32 cm (1/8"), and a standoff of 2.88 cm (1-1/8"). The results of all tests are shown in Table 5.

TABLE 5: RESULTS OF DEPTH OF PENETRATION TESTS AND SIMULATIONS WITH SMALL SCALE SHAPED CHARGES AGAINST GRAPHITE

Test	*Charge*	*Material*	*Standoff (cm)*	*DOP (cm)*	*Simulation DOP (cm)*
1	RP-1	PCEA	0.35	3.98	2.62
2	RP-1	PCEA	0.35	4.55	
3	RP-4	PCEA	0.32	10.24	
4	RP-4	PCEA	0.32	8.45	6.12
5	RP-4	PCEA	0.32	7.35	
6	RP-4	PCEA	2.86	6.87	
7	RP-4	PCEA	2.86	12.58	
8	RP-4	PCEA-Radial	2.86	12.34	12.03
9	RP-4	PCEA-Radial	2.86	9.41	
10	RP-4	NBG-18	2.86	10.1	10.46
11	RP-4	NBG-18	2.86	11.2	
12	RP-4	NBG-25	2.86	11.44	11.35
13	RP-4	NBG-25	2.86	11.12	

There may be a trend of decreasing penetration with increasing compressive strength. However, due to the small number of samples, the inherent variability in the tests, and the similarity between the materials, we cannot say with certainty that the penetration decreases with increasing compressive strength. One outcome of the tests was notably different. All PCEA shots remained intact, with no visible cracks emanating from the wound. However, one of the two NBG-18 tests and both NBG-25 tests split into two or three pieces after the test. After examination, it appears that the sample split happened behind the jet penetration. Combustion product residue appears to be on the crack surfaces behind the tip of the wound channel, but only about 2 cm ahead of it, as shown in Figure 6. This suggests that the crack finished propagating through the sample after the jet had stopped and the burn had completed. This is a reasonable conclusion, as the jet is moving faster than the speed of sound of the material, and the cracks are not likely to propagate that quickly.

FIGURE 6: IMAGE OF THE FRACTURED SURFACE FROM AN RP-4 SHAPED CHARGE PENETRATING NBG-25 GRAPHITE (TEST 13). THE JET MOVED FROM LEFT TO RIGHT. BURN RESIDUE IS FOCUSED ON THE CENTER OF THE SAMPLE.

The simulations with material model #1 had mixed results. The RP-1 simulation resulted in a DOP right in between the two experimental data points (4.368 cm, compare to Table 5). However, all RP-4 simulations (for all materials) resulted in complete penetration of the simulation boundary (over 18 cm).

The material parameters for material model #2 (JH2) were modified to obtain closely matching DOPs for the RP-4 cases. However, with this material model, the RP-1 case performs poorly. The material model does not seem to be able to capture the behavior of graphite against these different scales of shaped charges. The simulation results using the JH2 model are shown and compared to the test results in Table 5. Finally, note that the material model used would have overestimated the quasistatic or SHPB strengths by a factor of 5, yet these overestimated strengths are required for the model to achieve the DOP results observed in the experiments.

Note that the material model is not predictive in any case because the material parameters were essentially calibrated to obtain the desired DOP. However, we determined that the JH2 model could not represent the dynamic behavior of graphite. An appropriate material model needs to represent the energy dissipation mechanisms of graphite that occur prior to material failure.

3.3 Wound Channel Characteristics

The test of the JH2 model parameters is in the representation of the wound channel in the RP-4 cases. A representative simulation is shown in Figure 7. The simulation wound channel, based on the fully damaged material (taken as damage >= 0.99), averages about 1 cm diameter throughout the length of the wound. In contrast, the experimental samples show a wound channel diameter of about 0.3 cm, with a variation of about 0.05 cm between the different materials. Figure 8 shows a maximum intensity projection of an X-Ray computed tomography (XCT). The wound channel can be deduced from the brighter areas which represent copper. The wound channel is narrower than the shaped charge slug while in the simulation the wound channel is much larger.

In addition, the experiments showed a spall crater on the front face ranging from 1.3 to 1.9 cm in diameter. The simulations do not show any front spall, although the simulation region where the front spall would have occurred is completely cratered from the penetration event.

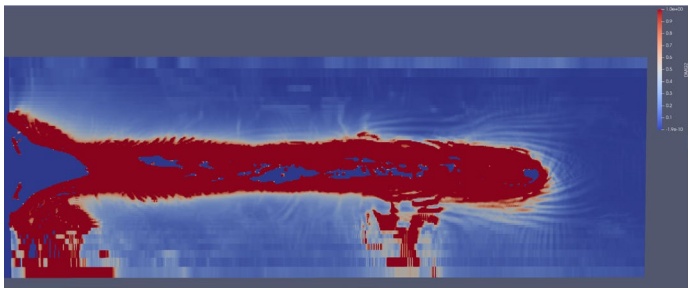

FIGURE 7: CONTOURS OF DAMAGE IN THE PENETRATION OF RP-4 INTO PCEA GRAPHITE WITH THE JOHNSON-HOLMQUIST II MODEL.

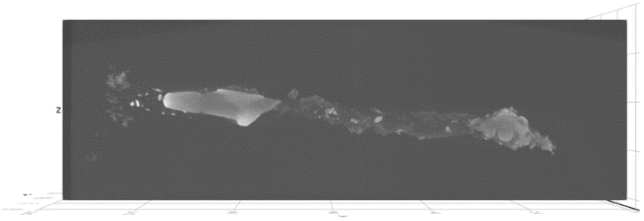

FIGURE 8: MAXIMUM INTENSITY PROJECTION OF X-RAY COMPUTED TOMOGRAPHY DATA FROM AN RP-4 SHAPED CHARGE PENETRATING PCEA GRAPHITE.

The inability of the modeling to consistently capture features of the penetration event is primarily attributed to the material models. The simulations may have produced better results if a full set of calibration experiments was performed for each of the grades of graphite. However, neither the JH2 model nor the GEO model are designed to represent graphite. Even with a fully calibrated model, differences would be expected. Two material behaviors are suspected to be important. First, graphite exhibits non-linear “elastic” behavior in compression due to its porosity. This behavior is termed “elastic” in the sense that, during a loading cycle, the stress and strain both return to zero. However, the stress exhibits a significant hysteresis, and the material dissipates energy during the loading cycle. This behavior could lead to the recovery of volumetric strain during the penetration event. Second, graphite exhibits shear localization behavior. Graphite next to the wound channels shows signs of compaction and shear failure, suggesting that the graphite could have created a localization effect where pores were closed and energy consumed, preventing failure from extending away from the wound channel as it does in the simulations.

4. CONCLUSION

A small-scale shaped charge penetrated up to 12.6 cm in a porous high purity graphite, PCEA. This provides the first published data for shaped charge DOP in graphite and should

provide useful information to modeling efforts for space applications. However, current material models are not predictive. Future work will need to better characterize the response of graphite to dynamic events and develop a model to capture unique material response of graphite.

ACKNOWLEDGEMENTS

This research made use of the resources of the High Performance Computing Center at Idaho National Laboratory, which is supported by the Office of Nuclear Energy of the U.S. Department of Energy and the Nuclear Science User Facilities under Contract No. DE-AC07-05ID14517.

REFERENCES

[1] Carroll, Mark Christopher, David Lynn Cottle, and David Thomas Rohrbaugh. *Data Report on the Newest Batch of PCEA Graphite for the VHTR Baseline Graphite Characterization Program*. No. INL/EXT-16-39604. Idaho National Lab.(INL), Idaho Falls, ID (United States), 2016.

[2] Carroll, Mark C. *Initial Comparison of Baseline Physical and Mechanical Properties for the VHTR Candidate Graphite Grades*. No. INL/EXT-14-33120. Idaho National Lab.(INL), Idaho Falls, ID (United States), 2014.

[3] Burchell, T. D., & Pavlov, T. R. (2020). “Graphite: properties and characteristics.”

[4] Yokoyama, T., Nakai, K., & Futakawa, M. (2008). “Compressive Stress-Strain Characteristics of Nuclear-Grade Graphite IG-11 Effects of Specimen Size and Strain Rate.” Transactions of the Atomic Energy Society of Japan, 7(1), 66-73.

[5] Yokoyama, T., & Nakai, K. (2014). “Dynamic Tensile Characteristics of Nuclear-Grade Graphite IG-11.” In Applied Mechanics and Materials (Vol. 566, pp. 61-66). Trans Tech Publications Ltd.

[6] Tian, D., Shi, L., Sun, L., Shen, K., & Xu, K. (2022, August). “Experimental Study on Dynamic Tensile Strength of Graphite.” In International Conference on Nuclear Engineering (Vol. 86366, p. V002T02A019). American Society of Mechanical Engineers.

[7] Diedrich, J. H., Loeffler, I. J., & Mc Millan, A. R. (1965). “Hypervelocity impact damage characteristics in beryllium and graphite plates and tubes” (No. NASA-TN-D-3018).

[8] Clough, N., Diedrich, J. H., & Lieblein, S. (1965). “Results of hypervelocity impacts into space radiator materials” (No. NASA-TM-X-52142).

[9] Jodar, B., et al. "Impacts into porous graphite: An investigation on crater formation and ejecta distribution." *International Journal of Impact Engineering* 152 (2021): 103842.

[10] Hebert, David, et al. "Plate impact experiments and simulation on porous graphite." *Journal of Physics: Conference Series*. Vol. 500. No. 18. IOP Publishing, 2014.

[11] Jaulin, Vincent, et al. "Laser-induced cratering of a 3DCC material at mesoscale: Experiments and simulations." *EPJ Web of Conferences*. Vol. 183. EDP Sciences, 2018.

[12] Grafstar datasheet. https://www.amstedgraphite.com/wp-content/uploads/2022/01/PCEA.pdf

[13] Kane, J., et al. "Microstructural characterization and pore structure analysis of nuclear graphite." *Journal of Nuclear Materials* 415.2 (2011): 189-197.

[14] Chi, Se-Hwan. "Comparison of the effects of irradiation on iso-molded, fine grain nuclear graphites: ETU-10, IG-110 and NBG-25." *Nuclear Engineering and Technology* 54.7 (2022): 2359-2366.

[15] Kim, Eung Seon, et al. "Porosity of Nuclear Gade Graphite." *Pro-ceedings of the KNS spring meeting, pages 1CD–ROM, Korea, Republic of*. 2012.

[16] Scheffler, Daniel R., Matthew S. Burkins, and William P. Walters. *Characterization of Jets from Exploding Bridge Wire Detonators*. Army Research Lab Aberdeen Proving Ground Md, Weapons and Materials Research Directorate, 2005.

[17] Teledyne Defense Electronics. “RP-4 SC EBW Shaped Charge.” https://www.teledynedefenseelectronics.com/energetics/Documents/RP-4SC_2020.pdf

[18] McGlaun, J. Michael, S. L. Thompson, and M. G. Elrick. "CTH: A three-dimensional shock wave physics code." International Journal of Impact Engineering 10.1-4 (1990): 351-360.

[19] Dafalias, F., and E. P. Popov. "A simple constitutive law for artificial graphite-like materials." (1975).

[20] Greenstreet, W. L., and A. Phillips. "A theory of an elastic-plastic continuum with special emphasis to artificial graphite." *Acta Mechanica* 16.1-2 (1973): 143-156.

[21] Spicer, James B., et al. "Laser ultrasonic assessment of the effects of porosity and microcracking on the elastic moduli of nuclear graphites." *Journal of Nuclear Materials* 471 (2016): 80-91.

[22] Johnson, Gordon R., and Tim J. Holmquist. "An improved computational constitutive model for brittle materials." *AIP conference proceedings*. Vol. 309. No. 1. American Institute of Physics, 1994.